FLIGHT CONTROL WITH MINIATURE TRAILING EDGE EFFECTORS

Stefan R. Bieniawski, Ilan M. Kroo
Stanford University, Stanford University

Keywords: *Flight Control, Flutter, Novel Actuators, Distributed Control*

Abstract

Recent developments in actuator technology have resulted in small, simple flow control devices capable of affecting the flow field over flight vehicles sufficiently to generate control forces. One of the devices which has been under investigation is the Miniature-Trailing Edge Effector (MiTE), which consists of a small, 1-5% chord, moveable surface mounted at the wing trailing edge. The high bandwidth, distributed placement, and good control authority make the device an ideal candidate for control of both the rigid body and flexible modes of a flight vehicle. This potential is demonstrated in two experiments: flutter suppression of a flexible wing, and flight control of a remotely piloted aircraft. The first experiment successfully increased the flutter speed by over 25%. The second experiment included a novel distributed flight control system based upon the MiTEs that includes distributed sensing, logic, and actuation. Flight tests were performed with conventional control surfaces and with the MiTE based distributed control system. These tests validated the control capability of the MiTEs and the associated flight control architecture. Controllers were then designed for the distributed flight control system. These controllers increased the flight vehicle stability by 85% and alleviated gust loads by 78%, when compared with open loop.

1 Introduction

Various actuation devices have been recently developed that can be used to locally affect the flow-field over flight vehicles [1, 2, 3, 4]. These devices modify the surrounding flow-field sufficiently to generate control forces. Often constructed using meso-scale or smaller manufacturing processes and utilizing a variety of actuation technologies, these devices are small in size, low in cost, and typically binary in nature. These new devices offer many potential advantages for flight vehicle control, including robustness due to the large number of devices, and simplicity through elimination of complicated servo-positioning. Furthermore, the high bandwidth and distributed placement of the new devices allows for structural as well as rigid body mode control. Application areas already considered for these devices include aircraft [2], helicopters [5], and wind turbines [6].

At Stanford University, research in small flow control devices began in 1998 and has focused on Miniature-Trailing Edge Effectors (MiTEs) [2, 7, 8]. The MiTEs are small trailing edge devices, approximately 1–5% chord in height, actuated with deflection angles up to 90 degrees. The MiTE concept is inspired by Gurney flaps originally developed and applied to racing cars by Robert Liebeck and Dan Gurney. These devices protrude vertically into the flow and cause a stable separation region to form [9], changing the sectional lift and moment comparable to a traditional flap of much larger size. Locating the MiTE at the trailing edge has the largest influence, although researchers have investigated other locations [5]. Numerous wind tunnel tests [5, 7, 8, 10, 11] and CFD simulations [7, 12, 13] have confirmed the influence and behavior of small flaps.

Although extensive aerodynamic testing has been completed with these types of small devices, researchers are only beginning to address their potential for active control. This paper describes the development of two experiments to demonstrate the potential of MiTEs for control. First, flutter of a flexible wing wind tunnel model is suppressed using MiTEs. Second, a novel flight control architecture based upon MiTEs is developed and implemented on a remotely piloted flight vehicle. The latter system is fully distributed, including sensing, logic, and actuation. This architecture can address many control challenges. For example, the large number of devices allows for tailoring of the lift distribution at off-design flight con-

ditions. The small, high-bandwidth devices can also alleviate gust loads, resulting in reduced structural weight. In addition, the devices allow for arbitrary combinations of control forces and are ideal for configurations such as flying wings.

2 Miniature-Trailing Edge Effectors

A summary of the key aerodynamic features, with a focus towards suitable modeling for control design, is provided by Lee [14]. A more detailed review of the available literature on MiTEs is provided by Solovitz [15]. Computational and experimental results [14, 15] have shown that MiTEs are effective in generating aerodynamic forces. The steady and unsteady behavior of the MiTEs can be modeled using linear thin airfoil theory [14]. Further, the effectiveness of the MiTEs scales almost linearly with respect to the device height and the spanwise length. In two-dimensional flow, a 1.5% chord vertically deflected device can change the section lift coefficient C_l by as much as 0.33 [14]. This is equivalent to deflecting a 10% chord conventional flap 8 degrees.

Many geometries and actuation schemes have been considered for the MiTEs [5, 7]. Two different designs were used for the current work, both utilizing electro-mechanical actuation. This type of actuation was selected for its simplicity, reliability, low voltage and power requirements, and high bandwidth. For the flutter experiment the vertically sliding MiTE design is used. The flight experimental platform uses two variants of the bucket type MiTE.

2.1 Vertically Sliding MiTE

This design consisted of a vertically sliding flap actuated by a direct-current (DC) pager motor. Figure 1 shows the individual components and the assembled MiTE. The MiTE actuators were manufactured in the Rapid Prototyping Laboratory by Byong-Ho Park using Shape Deposition Manufacturing [16]. Four of these MiTE actuators were arranged in two pairs to enable direct command of three states: up, neutral, and down. This was achieved by having one MiTE in each pair actuating from neutral to down and the other from neutral to up. The arrangement allowed for high bandwidth actuation and eliminated the need for a centering mechanism. For the flutter experiment, bandwidths of up to 40 Hz were achieved without any damage to the devices, despite extended duration tests.

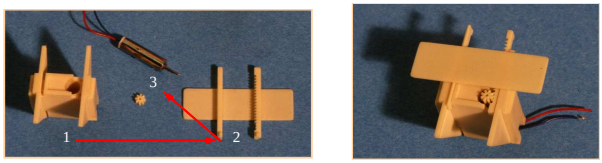

(a) Parts. (b) Assembled.

Fig. 1 Vertically sliding MiTE.

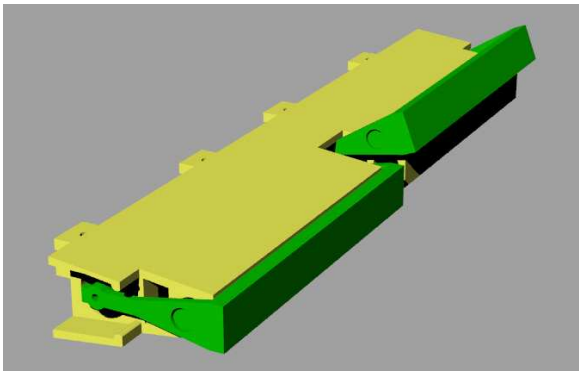

Fig. 2 Bucket type MiTE device.

2.2 Bucket Type MiTE

Two variants of the second type of MiTE device were utilized for the flight experiment. The first variant was configured into pairs, as with the vertically sliding MiTE, accomplishing four states. Two copies of the first type of device are shown side by side in Figure 2. The device consisted of two portions: a housing shown in yellow, and a moveable arm shown in green. The housing contained two DC motors for actuating the arm, which then influenced the aerodynamic flow. The arm ends were mounted directly to motor shafts, which were then driven in tandem to move the arm. Stops built into the housing constrained the allowable movement in a variety of combinations: movement from full up to full down, movement from neutral to down, or movement from neutral to up. The near device in Figure 2 is shown in the neutral position while the far device is in the up position.

The second variant of the bucket type design was capable of actuating to three distinct states: up, neutral, and down. The device remained simple, easy to manufacture, and highly reliable. The design consisted of two brackets each driven by DC motors located on each side of the housing. Each bracket can move to two positions, again limited by the geometry

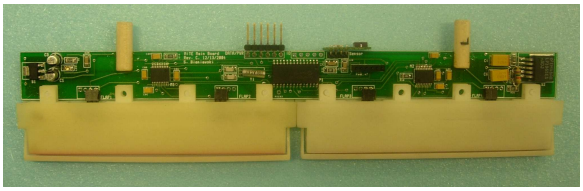

Fig. 3 Complete module including MiTEs and supporting electronics.

of the housing. The combination of these two positions allowed all three states of the arm to be commanded.

All components of both variants were manufactured using stereo-lithography to tolerances of 0.025 inches. The low required manufacturing tolerance was one of the advantages of the bucket type specific designs.

2.3 Supporting Electronics

Supporting electronics were developed to supply power to the devices, measure responses, implement control logic, and meet communication requirements. The goal was to develop supporting electronics that could fit into a space comparable in size to the devices themselves. This goal minimized the overall size of the modules in the control architecture, an especially critical requirement for the flight experiment. The core logic was built around the Microchip PIC family of microcontroller products.

For the second experiment the size and performance goals for the electronics were achieved as shown in Figure 3. Each module is comprised of two MiTE effectors, supporting logic and power conditioning circuitry, and an interface with a local sensor. The complete module measures 8.5 inches in length and 1.75 inches in depth. A bus interface provided two-wire communications and two types of raw power, one at 7.4 volts for the circuitry, the other at 3.7 volts for the DC motors that actuated the MiTEs. A microcontroller then provided the control logic to command several motor drivers that provided the actual voltage to the DC motors. Circuit design and manufacture of the supporting electronics were completed during the development of the flight experiment.

3 Flutter Suppression Experiment

3.1 General Description

To demonstrate the ability of the MiTEs to suppress aeroelastic instability and to illustrate novel approaches to control design, an experimental model was developed and equipped with sensors and MiTE actuators. An analytical model was developed in conjunction with the experimental model and used to validate the aerodynamic model of the MiTEs and develop controllers. The experimental model was designed to satisfy the flutter speed and frequency constraints of the MiTEs and of the wind tunnel facility. The design goal was a flutter frequency less than 5 Hz and a flutter speed of 15 m/s.

The primary structure of the experimental model was a laminated flat plate composed of 16 plies of wet-layup fiberglass fabric. The design was completed using the analytical model and consisted of varying the number of plies and the stacking sequence to obtain the desired flutter behavior. The final lamination sequence ensured the flutter mode was a combination of first bending/first torsion while also meeting the flutter speed and frequency goals. The mounting bracket for the model was manufactured to press-fit against the laminated plate, allowing the sweep to be varied. The variable sweep was used to separate the divergence and flutter modes, with the final configuration consisting of 5 degrees aft sweep.

Three sensors were placed on the laminated plate for measuring the response: a rate gyro, an accelerometer mounted midspan, and an accelerometer located near the wing tip. The locations of the MiTE actuators and sensors are shown schematically in Figure 4. An aerodynamic covering consisting of hot-wired EPP foam sections was also added to the upper portion of the model. Small gaps were cut between the sections of foam to avoid adding any torsional stiffness that would adversely affect the flutter characteristics. Figure 4(b) shows the final experimental model with MiTE actuators, sensors and foam covering.

Electronics were developed to process the sensor outputs, command the MiTE actuators, and archive the data. The microcontroller digitized the sensor readings, commanded the MiTEs, and transmitted all data to a PC through a RS-232 serial connection. The command and sensing cycle was limited to 122 Hz to allow sufficient time to transmit the serial data. The small size and low power consumption were obtained at the expense of the limited computational capability of the microcontroller. For this experiment, the com-

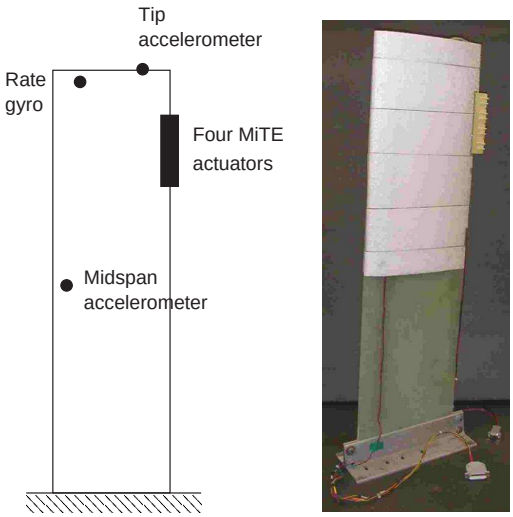

(a) Sensor and actuator locations.

(b) Final configuration.

Fig. 4 Aeroservoelastic experimental model.

putational capability was limited to integer math operations. As a result, a critical element of the controller designs was the complexity of the logic.

3.2 Open-Loop Testing

To obtain confidence in the analytical model for control synthesis, system identification tests were performed with the MiTEs commanded in a pseudo-random binary sequence [17]. Figure 5 shows the power spectra of the measured and predicted response at 14 m/s flow speed. The upper graph compares the rate gyro response, the middle compares the tip acceleration, and the lower shows the input. Good agreement was obtained at frequencies through 30 Hz. At higher frequencies, the accelerations differed, which was expected since only the first three modes were considered in the analytical model.

The sensor noise and disturbances were also characterized during open-loop testing. The sensor noise was modeled as Gaussian with zero mean and with the standard deviation obtained from test. The disturbance was modeled as a Gaussian control input with zero mean. A root mean square magnitude of 0.25 resulted in good agreement with the experiment.

The extensive open-loop testing confirmed that the analytical model can accurately predict the behavior of the experimental model. The testing also confirmed the modeling assumptions made for the

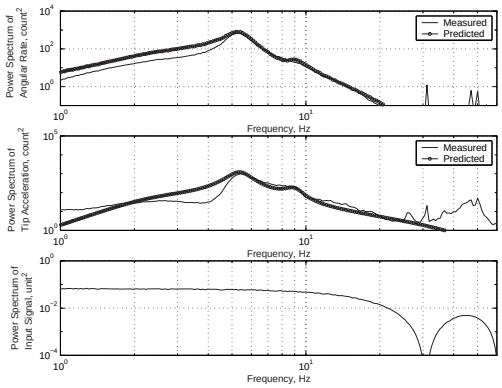

Fig. 5 Comparison of power spectra at 14 m/s flow speed.

MiTEs. The test verified analytical model was then used to perform controller synthesis to stabilize the system at flow speeds above the critical flutter speed.

3.3 Controller Synthesis

Pioneered for applications to Artificial Intelligence such as learning to play checkers and chess, Reinforcement Learning (RL) techniques are now widely used for developing controllers for general nonlinear, noisy systems [18]. RL provides a variety of approaches for control design, one of which is direct policy search. In this approach the control law is written in terms of a policy with a number of free parameters θ_i. The control synthesis then becomes an optimization of a defined objective function, typically a function of the measured states, with respect to these parameters. More details on this approach can be found in Bieniawski [19].

Policies were assumed to follow a threshold function,

$$u_i = \left\{ \begin{array}{ll} 1 & \theta^T Y \geq 153 \\ 0 & otherwise \end{array} \right\}, \qquad (1)$$

where $\vec{\theta}$ were the parameters governing the policies. The threshold of 153 provided scaling suitable for implementing the policies within the integer logic of the experimental software.

The controller design became the following unconstrained optimization,

$$\min_{\vec{\theta}} \hat{G}(\pi), \qquad (2)$$

subject to the system dynamics.

Optimal policies were determined using the Nelder-Meade nonlinear simplex [20] to minimize the

estimated objective function. This optimization approach was well suited for the current application because it did not require gradients and performed well for the low numbers of variables. Optimal policies were determined using this approach for a variety of flow speeds and feature sets. The two feature policy, utilizing the latest rate gyro and tip acceleration measurements, was able to stabilize the system through 18 m/s, and partially at 19 m/s.

3.4 Closed-Loop Testing

Closed loop tests were performed to demonstrate the MiTE control capability. The experimental model was mounted in the wind tunnel and the control policies programmed into the microcontroller. The first tests involved activating the controller at a flow speed above the critical speed, and suppressing the system response. The second tests explored the maximum controllable speed. These tests began with the controller on at a flow speed near the flutter speed. The flow speed was then increased until loss of control.

The optimal controller at 18 m/s was cycled at 16 m/s. The response is shown in Figure 6. Evident are the growth of the response with the controller off, and the eventual limit cycle due to aerodynamic and structural nonlinearities. The controller suppressed the response within 0.5 seconds with much higher actuation frequency than the simple rate gyro policy. Also evident is a higher residual acceleration response. A significant portion of this response was in frequencies above those considered in the analytical model and resulted primarily from the proximity of the sensor to the MiTEs.

3.5 Tests to Maximum Controllable Speed

Tests were performed to the maximum controllable speed using several different policies. Table 1 summarizes the results of these tests. The two feature controllers were successful at controlling the system through 19 m/s flow speed, increasing the flutter speed by 25%.

4 Flight Control Experiment

4.1 General Description of Flight Vehicle

A remotely piloted flight vehicle was developed to demonstrate the potential of novel distributed flight control architectures and to explore suitable control

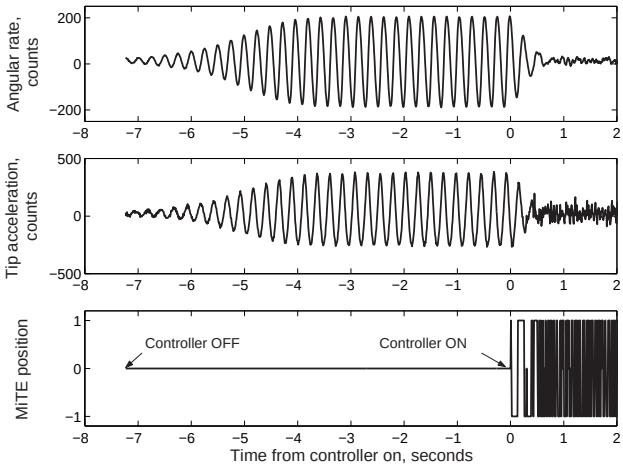

Fig. 6 Closed loop flutter suppression using MiTEs at 16.0 m/s.

Test	Sensor gains		Maximum
	Rate gyro	Tip accel.	speed
#1	32	10	19.35
#2	53	14	19.13
#3	23	6	19.13
#4	15	3	19.30

Table 1 Summary of tests to maximum controllable speed.

synthesis techniques. To enable comparisons, the vehicle can either be configured with four conventional servo-actuated control surfaces or with a MiTE-based distributed flight control system. The vehicle was a six foot span flying wing with 30 degrees of leading edge sweep. The outboard sections were of constant chord set to 12 inches to accommodate MiTEs with 2% chord deflected height. The wing skins were manufactured from balsa core sandwich panels faced with carbon fiber and fiberglass. The vehicle had an electric powerplant composed of an advanced external rotor brushless motor driving a 10-by-6 inch propeller drawing current from a three cell Lithium Polymer battery pack. The vehicle was designed to fly efficiently at an overall lift coefficient of 0.7 achieved with a combination of airfoil selection and wing washout. The flying weight of the conventional control configuration was 4.4 pounds.

The vehicle was tested in two configurations, free-flight and mounted to a car. In the latter configuration, the vehicle was prevented from displacing while being free to rotate about any axis. In all other respects, such as power, communication, and data acquisition, the

configurations were identical. For the car-top testing the vehicle was mounted at its center of gravity to a frame that was then attached to a car. This provided a much more controlled environment for evaluating the control system. The effects of the mounting on the vehicle dynamics were considered.

4.2 Distributed Control Architecture

The distributed control architecture is shown schematically in Figure 7. The key feature of the architecture were the individual "agents" or modules that were comprised of sensors, actuators, and logic. The pilot commands were received by the central microcontroller and then broadcasted to both the logging microcontroller and the distributed modules. This was accomplished through a communication and power bus running the length of the trailing edge. Power was provided to the distributed modules by centralized batteries, although the power supply could also be distributed through the airframe. The bus provided eight possible positions for the modules, including three positions in each outboard wing and two in the centerbody. A unique feature of the architecture was modularity: this allowed all the modules to be interchanged and supported "hot-plugging" between the different positions. Although the flight vehicle was relatively small, the architecture and hardware developed for this experiment can easily be scaled to a much larger vehicle with little modification.

A close-up view of a module mounted in one of the centerbody positions is shown in Figure 8. A detailed description of the modules, including the MiTE actuators and supporting electronics, is provided in Section 2.3. Each module was comprised of two MiTE effectors, supporting logic and power conditioning circuitry, and an interface with a local sensor. The MiTE devices were manufactured to conform to the trailing edge shape, leaving a clean aerodynamic surface when not actuated. The logic consisted of a microcontroller that combined the broadcasted pilot commands with the locally sensed data and commanded the positions of the MiTEs. For the closed-loop experiments described later, the local sensors consisted of single axis accelerometers although other sensors, such as pressure sensors, could be used for different applications.

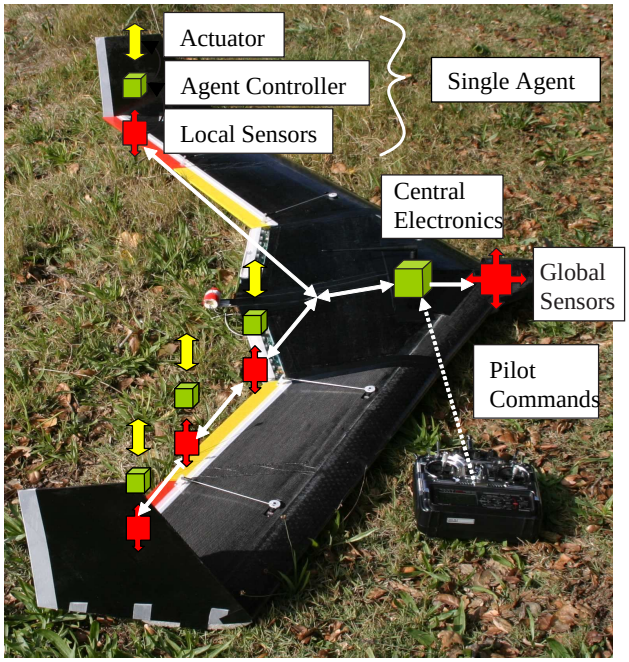

Fig. 7 Distributed flight control architecture.

Fig. 8 MiTE based "agent" in flight configuration.

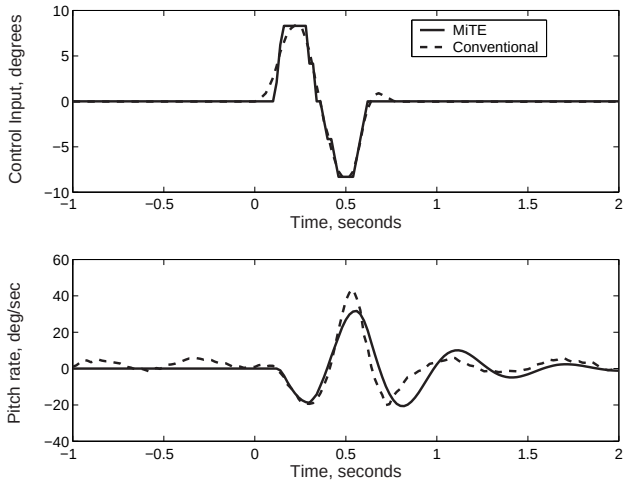

Fig. 9 Corrected comparison of longitudinal responses.

4.3 Open Loop Tests

Tests were performed to characterize the influence of the MiTEs and to validate the analytical models. A series of aileron and elevator doublets were completed with the vehicle in the captive car configuration and free-flight. The captive tests were completed using conventional servo-actuators and the MiTE based distributed control architecture. The tests verified the operation of the distributed control architecture and the data acquisition and logging system. The results also confirmed the influence of the MiTEs on the vehicle dynamics and their ability to generate sufficient control forces. Open loop free-flight tests utilized conventional actuators to validate the flight dynamic model. The resulting validated car-top and free-flight dynamic models were used during the controller synthesis. An example of the comparison is shown in Figure 9 for the longitudinal doublet. The data has been corrected for differences in the configuration.

Tests were performed to confirm the free flight dynamics of the vehicle. A series of aileron and elevator doublets were completed with the conventional servo-actuated control surfaces installed. Flight speeds were typically 11-12 m/s. The resulting data were used to validate the predictions from the analytical model. This validated model was then used for the synthesis of gust load alleviation controllers. Similar comparisons were also obtained for the lateral model.

4.4 Controller Designs

Two controllers were designed for the flight vehicle equipped with the distributed, MiTE-based, flight control system. Both designs were accomplished using the Probability Collectives approach described in Bieniawski [19]. The first controller augmented the stability of the complete vehicle in the car-top configuration. The second alleviated the longitudinal response to random vertical gusts.

4.4.1 Stability Augmentation

The objective of the first controller was to stabilize the combined vehicle lateral and longitudinal dynamics in the captive car configuration. The challenge with this controller design was to determine the optimal allocation of the nonlinear effectors to accomplish the objective. A typical linear controller design for this application would separate the modes, determine the optimal controller for each, and then linearly superimpose the control input. This type of controller would also likely require extensive communication between the various modules. In the approach taken here, each module determined its action based solely on its locally sensed vertical velocity. Through the control synthesis process, the allocation was determined without explicit coordination, while accounting for the nonlinearity of the effectors.

The control system is shown schematically in Figure 10. Each module i located in the outboard sections of the flight vehicle utilized the locally sensed vertical velocity y_i to accomplish the objective. In practice, this measurement could be obtained in several ways. One possibility is to integrate and filter the locally measured vertical accelerations. This approach was successfully implemented in the hardware and used in the closed loop testing described later. Alternatively, angular rate data from the Inertial Measurement Unit (IMU) could be broadcast, along with the pilot commands already provided, to each controller. With knowledge of their locations relative to the IMU, the controllers could compute their local vertical velocity.

The control input for each agent i, u_i, was given by a threshold policy parameterized by a weight θ_i,

$$u_i = \begin{Bmatrix} +1 & \theta_i^T y_i \geq 1 \\ +0.5 & 0.5 \leq \theta_i^T y_i < 1 \\ 0 & otherwise \\ -0.5 & -0.5 \geq \theta_i^T y_i > -1 \\ -1 & \theta_i^T y_i \leq -1 \end{Bmatrix}$$

The five possible commands resulted from combinations of the two MiTEs present in each module. The

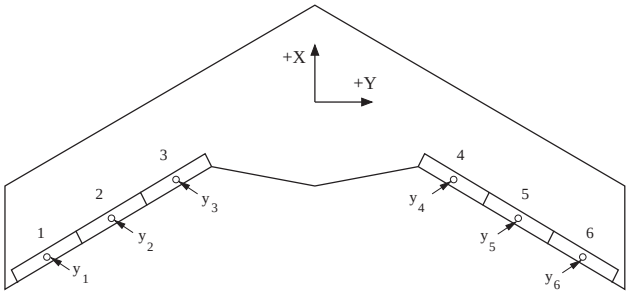

Fig. 10 Definitions for distributed stability augmentation controller.

command of $u_i = +1$ actuated both MiTEs within module i down while a command of +0.5 actuated only one down. The model assumed that the control input was independent of the MiTE that was actuated in the module.

The objective function was given by,

$$G(\vec{\theta}) = \sum_{k=1}^{T} \sum_{i=1}^{6} [y_i(k)]^2 \tag{3}$$

where the y_i at each time step k were obtained by simulating the discrete time vehicle equations of motion. A time horizon of $T = 5$ seconds was considered for each simulation.

The resulting optimization had six total variables and was performed in a distributed manner using the Probability Collectives approach [19]. Figure 11 compares the open loop and closed loop time histories for the vehicle angular rates. The controller dramatically decreased the initial pitch and roll responses and also decreased the yaw response. Note that the objective function, through the local vertical velocities, only included the roll and pitch rates. No explicit effort was therefore made to minimize the yaw rate. The reduction seen in Figure 11 resulted from coupling between the rates within the lateral oscillation mode.

4.4.2 Gust Alleviation

A second controller utilized the MiTE based distributed control system to minimize the longitudinal response, in flight, to random vertical gusts. The Probability Collectives approach was used to synthesize nonlinear, distributed controllers that were robust to the disturbances.

The control system is shown schematically in Figure 12. Since only the longitudinal response was considered, symmetry was enforced between the controllers on opposite wings. Two combinations of local

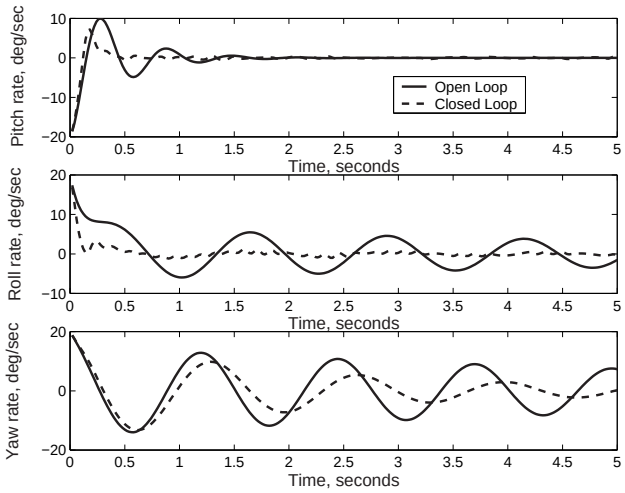

Fig. 11 Comparison of open and closed loop response.

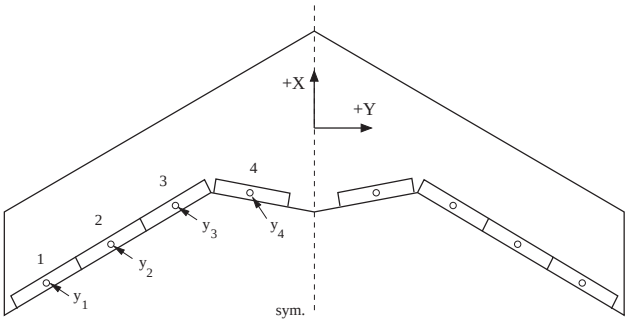

Fig. 12 Definitions for gust load alleviation controller.

measurements y_i were considered. First, each module i utilized the locally sensed vertical velocity to accomplish the objective. Second, each module utilized the local vertical velocity and acceleration to accomplish the objective. A variety of other possible measurements, such as changes in the local pressure, may also be effective for this type of controller. As mentioned during the description of the stability augmentation controller, the vertical velocity may be obtained through a variety of means. The details of obtaining these measurements, and the possible associated lags and uncertainties, were not considered in this work.

The objective function was given by,

$$G(\vec{\theta}) = \sum_{k=1}^{T} [\Delta RBM(k)]^2 \tag{4}$$

where ΔRBM was the increment to the root bending moment relative to steady level flight. This was modeled as a linear combination of the vehicle states and control inputs with coefficients obtained from the aerodynamic model. The gust dynamics were simu-

lated using the Dryden turbulence model [21]. A turbulence intensity of $\sigma_w = 1.0$ m/s was specified. The objective was evaluated by simulating the dynamic model over the time horizon with the control policies defined by Eqn. 4.4.1 and the parameter weights $\vec{\theta}_i$. For this controller, the weight vector for each module consisted of either one or two elements, depending upon the number of measurements used.

A second set of distributed controllers was designed utilizing the local vertical velocities and accelerations. With these measurements, the control objective was essentially to determine the optimal switching line within the local phase space of each module. The objective was therefore a generalization of bang-off-bang controllers often used for attitude control of spacecraft [22]. The goal with the controller was to further improve the performance by reducing high frequency input resulting from excessive switching. The first four variables specified the angle, in degrees, of the switching line in phase space within the range $[0, 360]$. The second four variables specified the width of the deadband on either side of the switching line. The allowable range was $[0, 50]$.

The optimal policies of the two types of controllers are compared in Figure 13. The control was primarily accomplished in both cases by modules 1, 3, and 4. The latter two acted typically in opposition to the first. Also note the relative angles of the switching lines. For module 4, the switching lines of the different controllers were almost orthogonal. The deadband for the velocity only controller was much smaller to correct for the difference in angle. This also likely resulted in excessive chatter, contributing to the higher frequency response.

The performance of the controllers was evaluated over an extended simulation of 5000 seconds. The best variants of both controllers are compared with the open loop in Figure 14. The upper curves compare the power spectra of the increment in the root bending moment. The lower curves then compare the running root mean square amplitude. The controllers significantly reduced the increments to the root bending moment at low frequency and slightly increased them at frequencies above 2 Hz. The increase was associated with the high frequency actuation of controller. The use of local acceleration, in addition to the local velocity, improved the performance over the complete range of frequencies. At the lower frequencies, the root bending moment was reduced by almost two orders of magnitude compared with the open loop. The

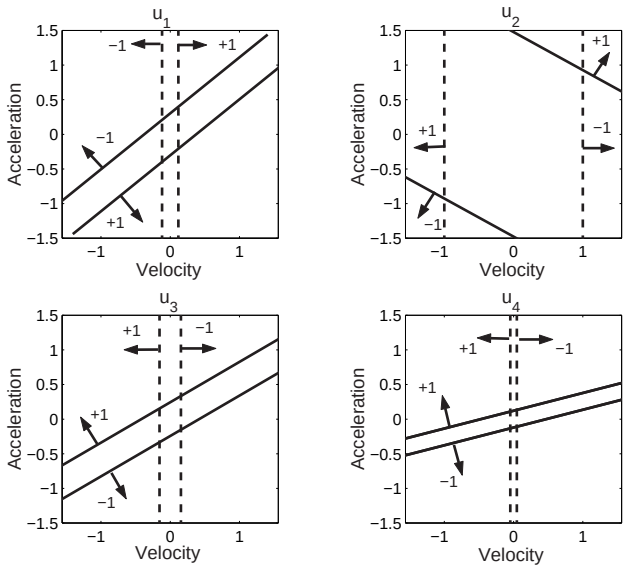

Fig. 13 Comparison of policies for the gust alleviation controllers.

root mean square responses were reduced by a factor of 2.9 and 5.5 by the four and eight variable controllers, respectively.

4.5 Closed Loop Tests

In the experiments, the two outboard modules were provided with local vertical accelerations. These were integrated and filtered by the microcontrollers within the modules to provide vertical velocities. A single gain value of $\theta = 1.75$ was applied to the local velocities. If the combined value exceeded a threshold of one or minus one, both MiTEs belonging to the agent were actuated in unison up or down, respectively. This was a simplified version of the policy used for the controller designs. Table 2 provides a comparison of the performance with the distributed controllers on and off. Listed are the root mean square values for the flight vehicle angular rates. A significant decrease in the response of the lateral mode was obtained, while the response of the longitudinal mode was increased slightly. These results are preliminary since many factors associated with the testing were not taken into account, including the source, magnitude, and consistency of the disturbances. While further testing is required to provide a more comprehensive comparison, the initial results are promising.

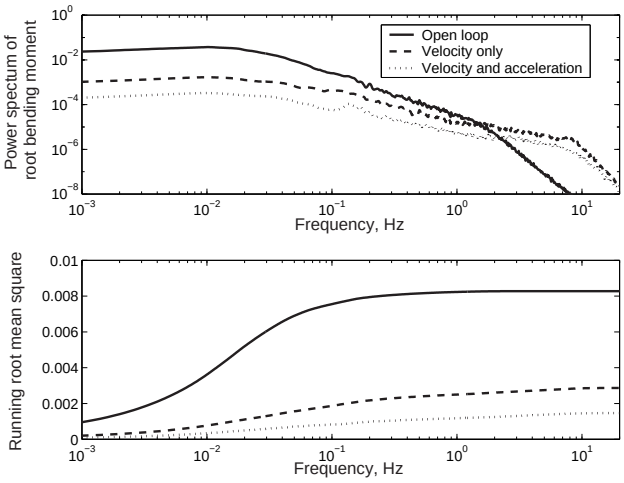

Fig. 14 Performance of the gust load alleviation controllers.

	Root mean square responses, deg/sec		
	Pitch rate	Roll rate	Yaw rate
Open loop	11.4	22.9	10.5
Closed loop	11.6	18.4	7.5
Difference	+2%	-20%	-29%

Table 2 Test results with distributed stability augmentation system.

4.6 Summary

A flight vehicle was developed with a distributed control architecture based upon Miniature Trailing Edge Effectors (MiTEs). Results of open-loop testing confirmed the influence of the MiTEs on the rigid body dynamics. Forces sufficient to perform primary flight control were generated. Open loop tests validated the analytical models subsequently used for control synthesis. Two types of controllers, one for stability augmentation and one for gust load alleviation, were developed for the flight vehicle. The resulting controllers illustrated the potential of a distributed architecture. The distributed stability augmentation controller coupled the lateral and longitudinal dynamics to reduce the response, compared with open loop, by 85%. Considering only the longitudinal dynamics, the gust load alleviation controller reduced the root mean square response to a random gust field by 78% compared with open loop. Results of initial closed loop tests with a simplified distributed stability augmentation system were also provided. A reduction in the lateral response of nearly 30% was observed.

5 Conclusions

Control of the flexible and rigid body modes of flight vehicles using MiTEs has been demonstrated through two separate experiments. The first experiment resulting in a 25% increase in the flutter speed of an experimental wing. The second demonstrated a flight control architecture based upon the MiTEs and illustrated distributed stability augmentation and gust load alleviation. The MiTEs and an associated control architecture offer the potential for significantly improving the performance of flight vehicle through their high bandwidth, distributed placement, and robustness.

6 Acknowledgements

The research was made possible by the financial support of the Air Force Office of Scientific Research, NASA Langley and Ames Research Centers, and the Boeing Company. The involvement of these different funding sources each provided an added dimension to this work and is greatly appreciated. The authors would also like to acknowledge the contributions of Dr. David Wolpert.

References

[1] A. M. Honohan, M. Amitay, and A. Glezer. Aerodynamic control using synthetic jets. In *Fluids 2000 Conference and Exhibit*, Denver, CO, June 19-22 2000. AIAA-2000-2401.

[2] I. Kroo. Aerodynamic concepts for future aircraft. In *30th AIAA Fluid Dynamics Conference*, Norfolk, VA, June-July 1999. AIAA 99-3524.

[3] C. Nae. Synthetic jet influence on NACA 0012 airfoil at high angles of attack. 1998. AIAA Paper 98-4523.

[4] A. Seifert, A. Darabi, and I. Wygnanski. Delay of airfoil stall by periodic excitation. *Journal of Aircraft*, 32(4), July-August 1996.

[5] M. Kinzel, M. Maughmer, and G. Lesieutre. Numerical investigation of miniature trailing-edge effectors on static and oscillating airfoils. In *43rd AIAA Aerospace Sciences Meeting and Exhibit*, Reno, Nevada, Jan. 10-13 2005. AIAA-2005-1039.

[6] D. T. Yen Nakafuji, C. P. van Dam, J. Michel, and P. Morrison. Load control for turbine blades - a non-traditional microtab approach. In *2002 ASME Wind Energy Symposium; 40th AIAA Aerospace Sciences Meeting and Exhibit*, Reno, NV, Jan. 14-17 2002. AIAA-2002-54.

[7] I. Kroo, J. Eaton, and F. Prinz. UAV aeroelastic control using redundant microflaps. Technical report, Air

Force Office of Scientific Research Program Review for Year I, 1999.

[8] S. Solovitz and J. K. Eaton. Aeroelastic control using redundant microactuators. In *3rd ASME/JSME Joint Fluids Engineering Conference*, San Francisco, CA, July 18-23 1999.

[9] R. H. Liebeck. Design of subsonic airfoils for high lift. *Journal of Aircraft*, 15(9), Sept. 1978.

[10] D. Jeffrey, X. Zhang, and D. W. Hurst. Aerodynamics of gurney flaps on a single-element high-lift wing. *Journal of Aircraft*, 37(2):295–301, 2000.

[11] B. L. Storms and C. S. Jang. Lift enhancement of an airfoil using a gurney flap and vortex generators. *Journal of Aircraft*, 31(3), June 1994.

[12] C. S. Jang, J. C. Ross, and R. M. Cummings. Computational evaluation of an airfoil with a gurney flap. June 1992. AIAA Paper 92-2708.

[13] H. Lee and I. Kroo. Computational investigation of airfoils with miniature trailing edge control surfaces. In *42nd AIAA Aerospace Sciences Meeting and Exhibit*, Reno, Nevada, January 2004. AIAA 2004-1051.

[14] Hak-Tae Lee. *Computational Investigation of Miniature Trailing Edge Effectors*. PhD thesis, Stanford University, 2005.

[15] S. Solovitz. *Experimental Aerodynamics of Mesoscale Trailing-Edge Actuators*. PhD thesis, Stanford University, 2002.

[16] Byong-Ho Park. *Design and Fabrication of Miniature Assemblies with SDM Processing*. PhD thesis, Stanford University, 2002.

[17] L. Ljung. *System Identification: Theory for the User*. Prentice Hall PTR, 1999.

[18] R. S. Sutton and A. G. Barto. *Reinforcement Learning*. MIT Press, 2002.

[19] S. Bieniawski. *Distributed Optimization and Flight Control Using Collectives*. PhD thesis, Stanford University, 2006.

[20] Philip E. Gill, Walter Murray, and Margaret H. Wright. *Practical optimization*. Academic Press, 1981.

[21] F. Hoblit. *Gust Loads on Aircraft: Concepts and Applications*. AIAA Education Series, 1988.

[22] A. Bryson. *Control of Spacecraft and Aircraft*. Princeton University Press, 1994.